Carbon Vol. 18, pp. 179–189

0008-6223/80/0601-0179/$02.00/0

OXIDATION EFFECTS ON TOUGHNESS AND SLOW CRACK GROWTH IN POLYCRYSTALLINE GRAPHITES

J. L. WOOD,† R. C. BRADT and P. L. WALKER, JR.

Department of Materials Science and Engineering, The Pennsylvania State University, University Park, PA 16802, U.S.A.

(*Received* 26 *September* 1979)

Abstract—The fracture toughness (K_{Ic}) and slow crack growth behavior of four fine-grained polycrystalline graphites, oxidized to 5, 10 and 20% weight losses, were measured in air at room temperature. Exponential decreases in the elastic moduli as well as decreases in the fracture surface energy contributed to lowering K_{Ic}. Oxidation generally shifted the stress intensity-crack velocity (K_I–V_I) diagram to lower stress intensity values, and decreased the slope, or N-value. Scanning electron microscope fractography revealed that a combination of filler particle and binder phase degradation with increasing oxidation was responsible for the decreased toughness and changes in the (K_I–V_I) characteristics. Oxidation conditions were shown to significantly affect the magnitude of decreases in the physical, elastic and mechanical properties of these graphites.

1. INTRODUCTION

In terms of the classical Griffith equation [1], which describes catastrophic failure in brittle materials:

$$\sigma_f = K_{Ic} c^{-1/2} Y \qquad (1)$$

where σ_f is the fracture stress, c is the flaw size, Y is a geometrical constant, and K_{Ic} is the fracture toughness, previous studies relating oxidation and the mechanical properties of graphites have been primarily concerned with the fracture stress, σ_f. In general, a number of studies have reported a 50% reduction in strength at weight losses ranging from as low as 6% to as high as 25% [2–6]. As is evident from eqn. (1), this strength decrease may be a combination of a fracture toughness, K_{Ic}, decrease and a flaw size, c, increase. The flaw size increase could occur during oxidation and/or be a consequence of subcritical or slow crack growth.

In some load bearing applications, however, the ultimate mechanical failure of the graphite may be governed by the rate of subcritical crack growth in the material. For these cases, the effects of oxidation on the toughness, K_{Ic}, and also on the slow crack growth behavior of the graphites must be documented and understood.

Strength measurements are insufficient to enable an understanding of the strength losses for they do not separate the K_{Ic} and c effects. In lieu of such data for oxidized graphites, the most useful information from oxidation-strength studies, therefore, is the effect of oxidation on the micromechanics of fracture, i.e. the extent of material degradation, the effects of preferential oxidation of the binder phase, and changes in the fracture path as a function of oxidation level.

Board and Squires [3], examining PGA graphite, found that fracture in unoxidized material occurs by crack propagation almost totally through the filler grains. However, cracks propagate predominantly in the binder or along the binder-filler interface in the oxidized material. Preferential oxidation and weakening of the binder phase was noted. In addition, some visible corrosion of larger filler particles was noted, taking the form of oxidation at surface striations, possibly microcracks. Rounthwaite *et al.* [4] reported failure in both as-received and oxidized PGA graphite to initiate by shear failure of the filler particles. Again, the binder phase was reported to be preferentially oxidized. In yet another study of PGA graphite, Knibbs and Morris [5] reported the binder or the binder-filler interface to be preferentially oxidized. Bognet [6] found similar preferential oxidation of the binder phase in Stackpole grade 2020 and Great Lakes H-440 materials and related that observation to exponential compressive strength reductions measured in those graphites.

The above investigations have established through oxidation-strength studies that oxidation generally degrades the mechanical properties of graphites through an alteration of the micromechanics of fracture. It is the objective of the present study to examine the effects of oxidation on the mechanical properties and microstructure of graphite, as that microstructure relates to subcritical crack growth and fracture toughness.

†Present address: Bendix Aircraft Brake & Strut Division, 3520 W. Westmoor Street, P.O. Box 10, South Bend, IN 46624, U.S.A.

2. EXPERIMENTAL PROCEDURE

Specimen preparation, characterization and mechanical property measurements for the four graphites have been previously discussed [7]. The double-torsion test [8] was used to measure the slow crack growth behavior and fracture toughness of the graphites. Specimens were cut from artifacts in the longitudinal (L) orientation for the extruded grade and in the transverse (T) and longitudinal orientations for the molded materials. These orientations have been previously described and depicted with respect to the parent artifacts and preferred basal plane alignment due to processing [7].

2.1 *Oxidation of samples*

In its two extremes, oxidation of graphite can occur uniformly throughout the material or almost totally at the surface. Preliminary experiments were conducted to determine the desirable oxidation conditions of the former type for the materials in this study. The objective was to select a temperature at which significant density gradients within the oxidized specimens were minimized, while maximizing the number of oxidized specimens obtained within a reasonable length of time. By comparing the reaction rate of powders and solid samples of each graphite at a given temperature, the extent of mass transport controlled oxidation was determined. Temperatures between 350 and 850°C were investigated, with significant mass transport control observed only above 550°C. In the interest of obtaining a maximum number of samples, the oxidation temperature of 500°C was selected. This temperature produced an approx. 20% weight loss in the grade of lowest reactivity during a 168 hr (1 week) exposure to air.

Surface finished specimens (100-grit diamond wheel) were oxidized in a horizontal mullite tube furnace with dry air continuously introduced at a flow rate of 0.04 l/min. The graphite specimens (76 mm × 25 mm × 6 mm) were placed on edge in an alumina boat positioned within the furnace to be located entirely in the constant-temperature hot zone. Temperatures were measured and maintained by use of a controller equipped with a calibrated platinum vs platinum-10% rhodium thermocouple. Specimen weights were intermittently measured by removing the specimens and permitting a 20 min cooling period prior to weighing. To minimize oxidation variations between specimens, the individual specimen locations were changed following each weighing. No surface grinding of the specimens was necessary following the oxidation. In fact, there were only very minor changes in the surface appearance and external dimensions of the specimens.

3. RESULTS AND DISCUSSION

3.1 *Oxidation characterization*

Total burn-off rates for each graphite at 500°C, calculated as the weight loss per hour are tabulated in Table 1. The reactivity of the lampblack-filled grade, 4029, is higher than those of the petroleum coke grades at all burn-offs. As discussed by Walker *et al.* [9] differences in reactivity can be attributed to one or more of the following factors: (i) differences in the concentration of active sites, (ii) differences in the accessibility of reactant gas to these sites, and (iii) differences in the amount and activity of inorganic impurities present, which may act as catalysts. The higher reactivity of the lampblack-filled grade is consistent with its possessing the smallest crystallite size (highest concentration of active sites) and the largest open pore volume (highest accessibility of reactant gas to the active sites).

Two criteria were utilized to assess the uniformity of oxidation within the samples. First, the relative weight change, Δw (%), was compared with the relative change in apparent density, $\Delta\rho$ (%) (Table 1). For uniform oxidation throughout the specimen, $\Delta\rho = \Delta w$. That is, oxidation is proceeding so slowly that the concentration gradient of reactant across the specimen required to supply the reactant gas to the interior of the sample is insignificant. This is, by definition, Zone I [9]. As the oxidation rate increases, the concentration gradient of the reactant across the specimen monotonically increases, resulting in increasing non-uniformity of oxidation from the surface to the center of the specimen. At sufficiently high concentration gradients, oxidation can result in some decrease in sample volume as well as a decrease in density of the remaining specimen. In this case, $\Delta\rho < \Delta w$. In the limit, there is no decrease in density

Table 1. Information on air oxidation of graphites at 500°C

Grade	Burn-off Rate (%/hr)	-5% Total Burn-Off			-10% Total Burn-Off			-20% Total Burn-Off		
		Δw(%)	Δρ(%)	(1-Fe)	Δw(%)	Δρ(%)	(1-Fe)	Δw(%)	Δρ(%)	(1-Fe)
580	0.14	5.0	0.4	0.06	10.3	2.3	0.20	19.7	12.4	0.48
3499	0.23	6.0	0.6	0.08	9.8	4.7	0.33	19.8	15.5	0.48
KK-16	0.15	4.9	0.7	0.1	10.6	6.2	0.38	21.3	16.8	0.62
4029	0.44	4.7	0.4	0.06	10.5	3.4	0.29	19.8	9.2	0.44

of the remaining specimen, i.e. $\Delta\rho = 0$; and sample burn-off is completely accounted for by the decrease in sample volume. Results in Table 1 show that for each sample, at each total burn-off, $\Delta\rho < \Delta w$. That is, some fraction of the total burn-off is accounted for by a reduction in sample volume (complete removal of carbon).

The second criterion, applied to the uniformity of oxidation, involved calculation of the fractional external burn-off (F_e) from the volumes of the as-received (V_0) and the oxidized specimens (V), the respective masses, m_0 and m, and the as-received density, according to:

$$F_e = \frac{(V_0 - V)\rho_0}{(m_0 - m)}. \quad (2)$$

The term $(1 - F_e)$, then, is the fraction of the total burn-off which occurred within the specimen interior. Values of $(1 - F_e)$ are given in Table 1. Using this approach, the percentage of weight loss which occurred in the remaining specimen, a measure of the amount of internal oxidation, can be calculated. For example, for grade KK-16 at 21.3% total burn-off, the weight loss in the remaining specimen was 13.2% (0.62 × 21.3%).

It is seen that the fraction of the total oxidation which occurred in the remaining specimen increases sharply with total burn-off. There are a number of possible reasons for this, including: (i) enlargement of the average pore and aperture size in the specimen during oxidation which leads to enhancement of the diffusion rate of the reactant into the pore system, (ii) the presence of a very reactive material at the surface of the specimen due to a concentration of inorganic impurities and/or mechanically deformed carbon debris (produced by the machining and polishing operations), and (iii) the existence of a denser layer at the surface, again as a result of the machining and polishing operations.

3.2 *Elastic moduli*

Young's elastic moduli, (E), shear moduli, (G), and Poisson's ratio, (ν), of the oxidized specimens were measured by the resonance technique [10]. In general, moduli decreases of about 20, 40 and 75% were observed for total weight losses of about 5, 10 and 20% respectively. Moduli, normalized to the as-received values, are plotted as a function of burn-off in the remaining specimen in Fig. 1. Of particular interest in Fig. 1 is the significant decrease in moduli for the rather negligible oxidation of the specimens, occurring during the initial 5% burn-off. Also, decreases in the normalized moduli are essentially independent of graphite grade.

Significant Poisson's ratio decreases were also evident. Applying the research results of Budiansky and O'Connell [11], these changes in Poisson's ratio can explain, in part, the moduli decreases with increasing burn-off. Their theory estimates the effective elastic moduli of a body permeated by many, randomly-

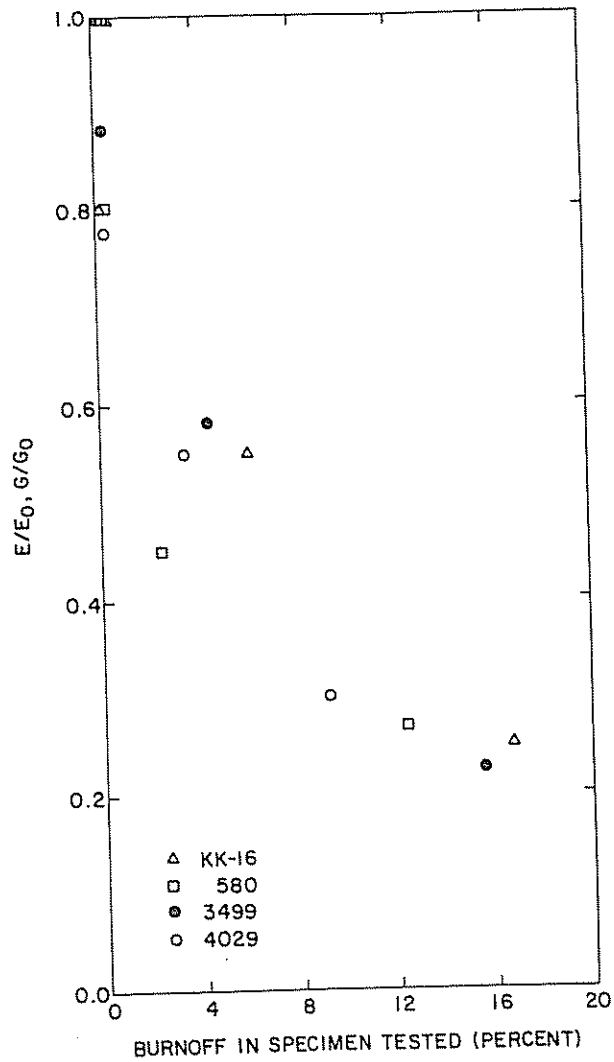

Fig. 1. Normalized moduli of the oxidized graphites as a function of burn-off (%) in the specimen tested.

distributed flat cracks, microcracks. In addition, their model assumes that the microcracked body is isotropic and homogeneous on a macroscopic scale. Although these conditions are not strictly fulfilled by the graphites of this study, the approximate change in E can be estimated from this self-consistent approach and the extent to which oxidation-produced microstructural changes actually function as microcracks can be ascertained. After Budiansky and O'Connell, the ratio of the elastic modulus of the body with long rectangular microcracks (E^*) to that of an uncracked body (E) is:

$$\frac{E^*}{E} = 1 - \frac{\pi^2}{30}(1 - \bar{\nu})(5 - 4\bar{\nu})\delta \quad (3)$$

where $\bar{\nu}$ is Poisson's ratio of the body with microcracks and δ is a crack descriptive parameter which can be calculated directly from the crack induced change in Poisson's ratio from:

$$\delta = \frac{60(\nu - \bar{\nu})}{\pi^2(1 + \bar{\nu})[10\nu - \bar{\nu}(1 + 8\nu)]} \quad (4)$$

where ν is Poisson's ratio of the uncracked body. In

Table 2. Normalized moduli (eqn 3) and measured values for the longitudinal orientation of grades 3499 and 4029

	E/E_o		G/G_o	
Grade/Total Burn-Off	Predicted	Measured	Predicted	Measured
3499/5%	0.89	0.88	0.91	0.88
3499/10%	0.77	0.58	0.78	0.58
3499/20%	0.43	0.22	0.44	0.22
4029/5%	0.75	0.77	0.75	0.77
4029/10%	0.66	0.55	0.67	0.55
4029/20%	0.48	0.29	0.48	0.29

this study, ν is taken as the as-received Poisson's ratio and $\bar{\nu}$ is Poisson's ratio of the oxidized specimens. Normalized moduli decreases predicted by this approach are compared with measured values in Table 2. At 5% burn-off, agreement between the measured and predicted values is excellent. Thus, it appears that some slight internal oxidation, undetected by the bulk density measurements, is occurring during the initial 5% burn-off, resulting in the production of microcrack-like internal defects. At higher oxidation levels, the measured values decrease more severely than the predicted values due to increased internal oxidation and resultant porosity. No consistent decrease in the measured Poisson's ratio is observed for oxidized grades KK-16 and 580 or the oxidized transverse specimens of 3499 and 4029, prohibiting analysis by the Budiansky and O'Connell approach.

The moduli of the oxidized grades, as a function of fractional total porosity, are adequately described by the empirical relationship:

$$Y = Y_0 e^{-bP} \tag{5}$$

where Y is the measured modulus, Y_0 is the extrapo-

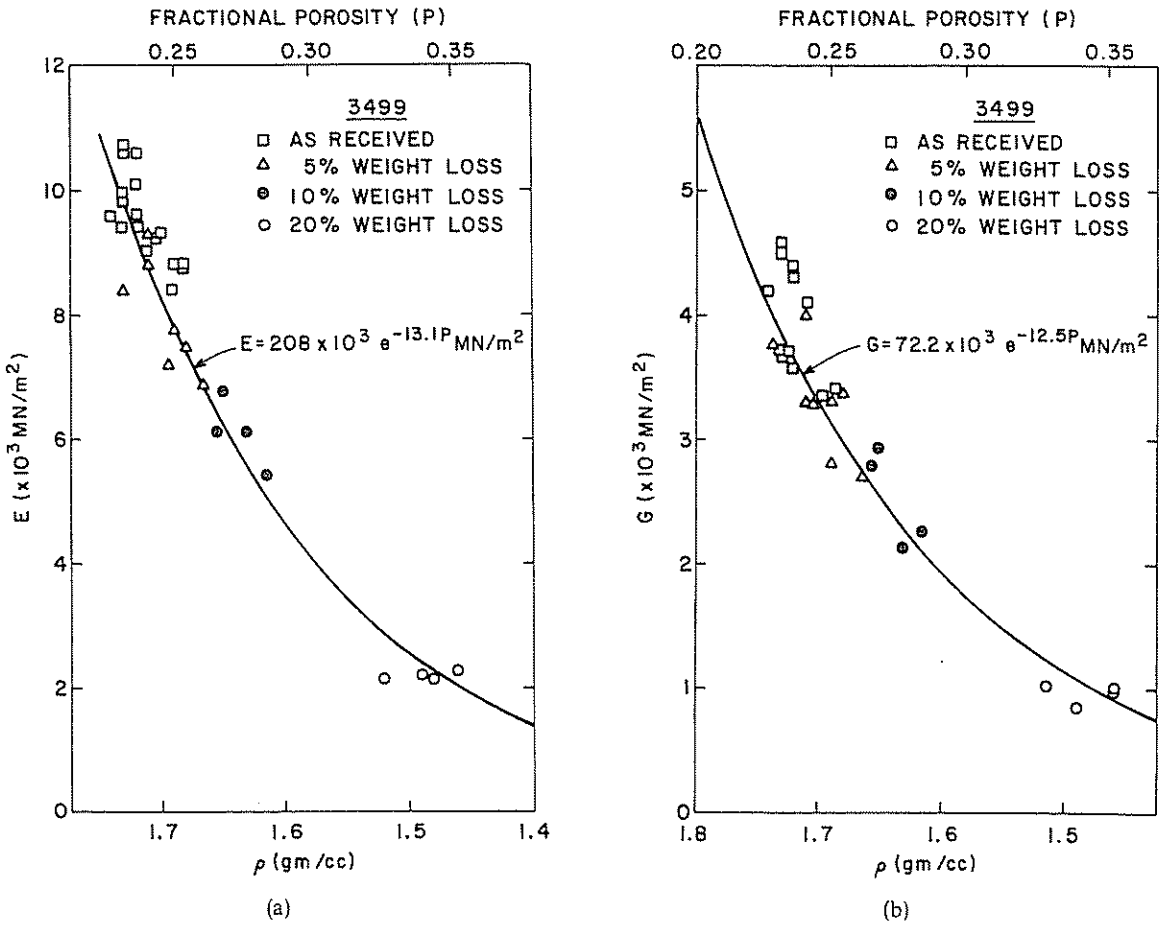

Fig. 2. (a) E as a function of fractional porosity and sample density for as-received and oxidized grade 3499. (b) G as a function of fractional porosity and sample density for as-received and oxidized grade 3499.

Table 3. Extrapolated moduli and exponential factor (eqn 5) of the oxidized graphites

Grade	Porosity Range (%)	Moduli are ($\times 10^{-4}$ MN/m^2) E	G
580	22–34	$b = 17.1$	$b = 17.9$
		$E_o = 75.7$	$G_o = 36.5$
3499	22–35	$b = 13.1$	$b = 12.5$
		$E_o = 20.8$	$G_o = 7.2$
KK-16	17–34	$b = 9.1$	$b = 9.3$
		$E_o = 6.2$	$G_o = 2.9$
4029	32–43	$b = 13.3$	$b = 12.8$
		$E_o = 43.7$	$G_o = 15.1$

lated zero-porosity value, b is a constant and P is the total fractional porosity. Data for E and G of grade 3499 are illustrated in Figs 2(a) and 2(b) respectively. The least squares regression line of the data fitted to eqn (5) is also shown on each diagram. The moduli, extrapolated to zero-porosity, and the exponential factors, b's, for all of the graphites, are shown in Table 3. The b values, ranging from 9.1 to 17.9, are 2.5–5 times larger than the value of 3.4 reported by Cost *et al.* [12] for specimens manufactured with varying porosity levels. It is concluded that the decrease in moduli produced by the introduction of porosity by oxidation appears to be 2.5–5 times more severe in elastic modulus reduction than that due to porosity controlled by processing variables.

The maximum and minimum values of elastic moduli for pore-free polycrystalline graphites can be estimated from single crystal stiffnesses [13] by using the Voigt constant-strain model [14] or the Reuss constant-stress model [15]. The extrapolated zero-porosity moduli of the graphites of this study (Table 3) are approximately equal to the Voigt value of 5.3×10^5 MN/m^2 and considerably exceed the Reuss value of 1.7×10^3 MN/m^2. The best averaging scheme for the moduli of the graphites of this study, therefore, would be one weighted in favor of the Voigt model, rather than the Reuss model. Cost *et al.* [12] reached similar conclusions for other graphites.

3.3 *Fracture*

3.3.1 *Fracture toughness.* The fracture toughnesses, K_{Ic}'s, of the oxidized graphites, are listed in Table 4. In general, K_{Ic} decreases of approx. 25, 50 and 70% occur for burn-off levels of 5, 10 and 20% respectively. The K_{Ic} decrease is substantial, consistently nearly 50% for only a 10% burn-off. Studies of the strength of oxidized graphite have frequently reported a 50% strength reduction for a 10% burn-off [2–4, 6]. Recalling that K_{Ic} and σ_f are directly related in eqn (1), it is apparent that the total strength reduction can be attributed solely to a decrease in K_{Ic}, i.e. the flaw size, c, does not necessarily increase during the oxidation process. Thus, the K_{Ic} data of this study strongly support the contention that decreases in the strength of oxidized graphite are primarily due to corresponding decreases in fracture toughness, not increases in intrinsic flaw size.

$\mathcal{G}_{Ic}$'s, critical strain-energy-release-rates (equals $2\gamma_f$, where γ_f is the fracture surface energy), are tabulated in Table 4. This parameter reflects the total energy required to create 1 m^2 of primary crack surface, including the energy consumed by all phenomena occurring in the process zone surrounding the advancing crack tip. These polycrystalline values are in agreement with those reported by Freiman *et al.* [16] for POCO AXF-5Q graphite. The polycrystalline values are substantially higher than reported graphite single crystal surface energies of 0.15 J/m^2 for graphite basal planes in air [17, 18] and 6 J/m^2 for crystal surfaces perpendicular to the graphite basal planes [18]. The higher energy demands in the polycrystalline material can be attributed, in part, to the creation of non-basal surfaces and crack branching or microcracking in the process zone. In general, $\mathcal{G}_{Ic}$ decreases of about 30, 50 and 65% are observed for burn-offs of about 5, 10 and 20% respectively. Some decreases in $\mathcal{G}_{Ic}$ for the 10 and 20% weight losses correlate with the apparent density, consistent with a

Table 4. Fracture toughness, K_{Ic} (MN/m$^{3/2}$), and critical strain-energy-release rate, $\mathcal{G}_{Ic}$ (J/m^2), of the oxidized graphites

Total Burn-Off %	As-Received		~5%		~10%		~20%	
Grade/Orientation	K_{Ic}	$\mathcal{G}_{Ic}$	K_{Ic}	$\mathcal{G}_{Ic}$	K_{Ic}	$\mathcal{G}_{Ic}$	K_{Ic}	$\mathcal{G}_{Ic}$
580 L	1.19	91	0.76	61	0.43	29	0.09	26
3499 L	1.00	95	0.81	72	0.57	52	0.27	32
3499 T	1.18	160	0.88	92	0.63	59	0.30	43
KK-16 L	1.33	155	1.06	120	0.68	87	0.52	68
KK-16 T	1.41	162	1.08	114	0.70	90	0.49	67
4029 L	0.50	38	0.40	52	0.32	33	0.19	21
4029 T	0.58	85	0.42	44	0.35	46	0.23	36

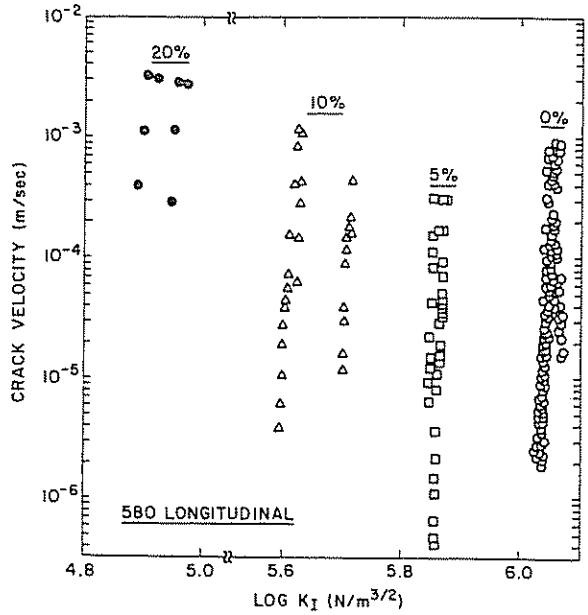

Fig. 3. Slow crack growth in as-received and oxidized grade 580.

simple mechanical failure model. That is, as the density decreases, the amount of material occupying the area of the fracture surface also decreases, requiring less energy to propagate the crack through a unit area whose density of atomic bonds is lowered correspondingly.

Increases in $\mathcal{G}_{Ic}$ for the longitudinal orientation of grade 4029 at 5% weight loss and the absence of a decrease from 5 to 10% weight loss for the transverse orientation of the same material are due to extensive microcrack formation in the binder phase during crack propagation. This is an interesting phenomenon in that the process zone around the advancing crack tip exhibits extensive microcracking. As a consequence, in spite of material degradation and density decreases, more energy is required for crack propagation, due to energy consumed by the formation of these microcracks. For these cases, however, K_{Ic} consistently decreases, primarily reflecting the severity of the exponential decrease in Young's elastic modulus during oxidation. This $\mathcal{G}_{Ic}$ increase also illustrates an obvious inconsistency in applying the simple mechanical model previously suggested.

3.3.2 *Subcritical crack growth.* Slow crack growth characteristics of the oxidized graphites for each oxidation level are readily presented in terms of stress intensity-crack velocity (K_I–V_I) diagrams. ($\mathcal{G}_I$–V_I) diagrams are equally valid. The (K_I–V_I) diagram for grade 580 is shown in Fig. 3. As previously reported for numerous graphites [16, 19], only a single region of stress intensity-crack velocity behavior is observed for this grade upon oxidation. This single region of slow crack growth can be described by:

$$V_I = AK_I^N \tag{6}$$

where V_I is the crack velocity, K_I is the stress intensity factor, and A and N are constants, with N equal to the slope of the line. For grade 580 following oxidation, the region is characterized by decreasing K_I's and decreasing N-values with increasing oxidation. At each oxidation level, slow crack growth is detected only at stress intensity factors which are large fractions (>0.90) of the respective K_{Ic}'s. These results suggest that the slow crack growth measured in oxidized grade 580 is primarily determined by mechanical failure (Region III), rather than by any stress corrosion mechanism (Region I).

The toughness of grade 580 decreases by more than an order of magnitude, from 1.19 MN/m$^{3/2}$ for the as-received material to only 0.09 MN/m$^{3/2}$ at the 20% weight loss level. It is apparent that the stress intensity necessary for slow crack propagation in grade 580 also decreases with increasing burn-off (Fig. 3). The fractional decrease is largest from 10 to 20% burn-off (note the break in the stress intensity abscissa), reflecting the increased amount of internal oxidation at the highest burn-off. For 580, the slope of the (K_I–V_I) diagram, the N-value, decreases from 215 ± 14 in the unoxidized material to 164 ± 21 at 5% total burn-off, to 68 ± 9 at 10% total burn-off, and finally to only

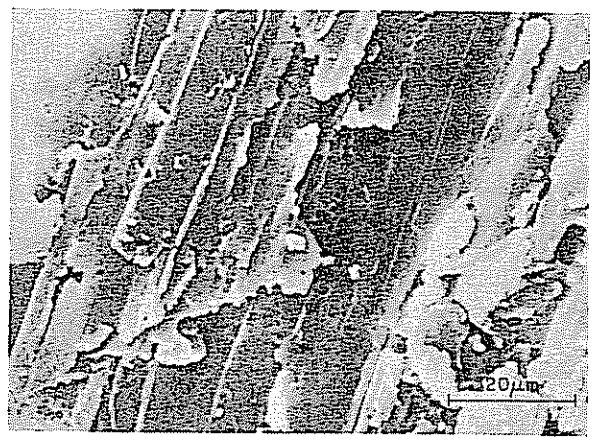

(a)

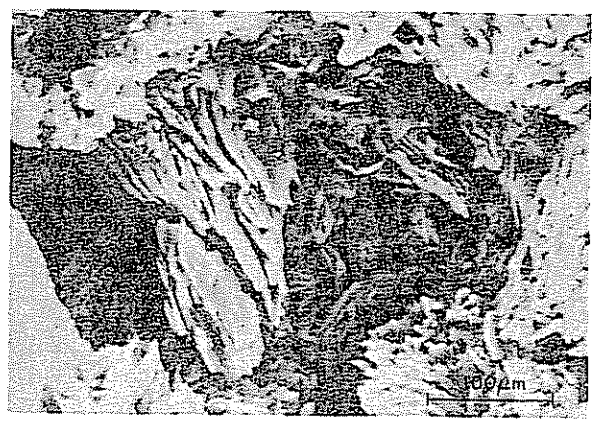

(b)

Fig. 4. (a) Cleavage of filler particle in longitudinal fracture surface of grade 580 oxidized to a total burn-off of ~20%. (b) Delamination of filler particles in longitudinal fracture surface of grade 580 oxidized to a total burn-off of ~20%.

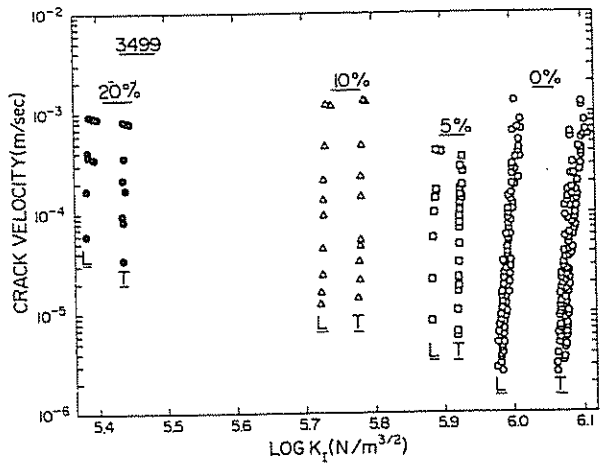

Fig. 5. Anisotropy of slow crack growth in as-received and oxidized grade 3499.

28 ± 36 at 20% total burn-off. This material clearly indicates the general trend of decreasing K_I for subcritical crack growth as well as decreasing N-value with increasing internal oxidation.

SEM fractographs reveal the material degradation responsible for the N-value and the fracture toughness decreases. Crack propagation in oxidized grade 580 occurs by a combination of cleavage of the large, degraded filler particles (Fig. 4a), delamination of the filler particles (Fig. 4b), and binder phase failure. Oxidation degradation of the filler particles, evident at the 10 and 20% oxidation levels, is characterized by channels, serrated edges, microcracks and circular etch pits. Substantial oxidation of the binder phase has also occurred as evidenced by the absence of binder phase on the fracture surfaces.

Variability in slow crack growth between the individual specimens of grade 580 also appears to increase with increasing oxidation. In Fig. 3, it is apparent that different specimens at 5% burn-off virtually coincide, similar in variability to the as-received material. At the 10 and 20% oxidation levels, however, distinct lines are obtained for individual specimens, perhaps reflecting some heterogeneity in the oxidation process that subsequently affects the slow crack growth character. As will be seen, this variability in K_I–V_I plots, following oxidation to 10 and 20% levels, was not found for the three molded grades.

The remaining three grades also exhibit only a single region of slow crack growth behavior in the oxidized state. For these grades, from two to six samples were measured in each orientation at each oxidation level. In general, they are also characterized by decreasing K_{Ic}'s (Table 4) and decreasing N-values with increasing burn-off (Table 5). The single regions of slow crack growth also occur only at large fractions of the respective K_{Ic}'s (0.56–0.84), indicating that the mechanism is primarily mechanical failure. For the three grades, 3499, KK-16 and 4029, the effect of increasing oxidation on slow crack growth anisotropy can also be ascertained; that is, differences in slow crack growth behavior between the transverse and longitudinal orientations.

Significant decreases in the stress intensity necessary for slow crack growth due to increasing oxidation are observed for both orientations of grade 3499 (Fig. 5). The fractional decrease is again largest over the 10 to 20% oxidation range, probably due to increasing amounts of internal oxidation at the 20% level.

Anisotropic slow crack growth behavior in grade 3499 is observed for all oxidation levels with the transverse orientations consistently tougher than the corresponding longitudinal orientations. Examination of the fracture surfaces reveals the crack front-microstructural interactions responsible for this anisotropy and, for the transverse orientation, reveals a distinct difference in crack path between the oxidized and the as-received materials. Crack propagation in the longitudinal orientation of the oxidized specimens

Table 5. Slow crack growth parameters, N, ($m^{5/2}$/MN·sec) and (log A) for the oxidized graphites

	As-Received		~5% Total Burn-Off		~10% Total Burn-Off		~20% Total Burn-Off	
Grade/Orientation	N	log A	N	log A	N	log A	N	log A
580 L	215 ± 14	−1304 ± 84	164 ± 21	− 966 ± 125	68 ± 9	− 384 ± 48	28 ± 36	− 142 ± 175
3499 L	198 ± 10	−1192 ± 61	106 ± 41	− 628 ± 244	128 ± 38	− 740 ± 217	79 ± 46	− 428 ± 247
3499 T	149 ± 13	− 909 ± 80	146 ± 21	− 868 ± 126	169 ± 37	− 983 ± 216	109 ± 66	− 598 ± 357
KK-16 L	152 ± 27	− 933 ± 164	178 ± 42	−1070 ± 254	138 ± 22	− 807 ± 129	134 ± 30	− 771 ± 168
KK-16 T	298 ± 22	−1836 ± 133	184 ± 35	−1112 ± 210	125 ± 25	− 733 ± 147	68 ± 17	− 388 ± 97
4029 L	224 ± 29	−1270 ± 165	112 ± 33	− 622 ± 181	122 ± 60	− 670 ± 327	60 ± 65	− 319 ± 341
4029 T	185 ± 12	−1067 ± 67	144 ± 20	− 640 ± 110	97 ± 39	− 538 ± 214	89 ± 74	− 482 ± 396

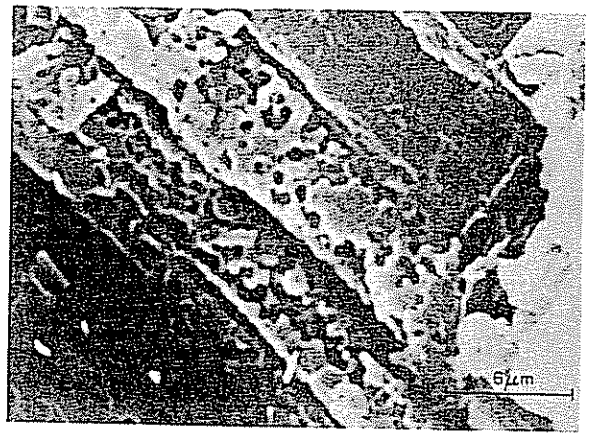

(a)

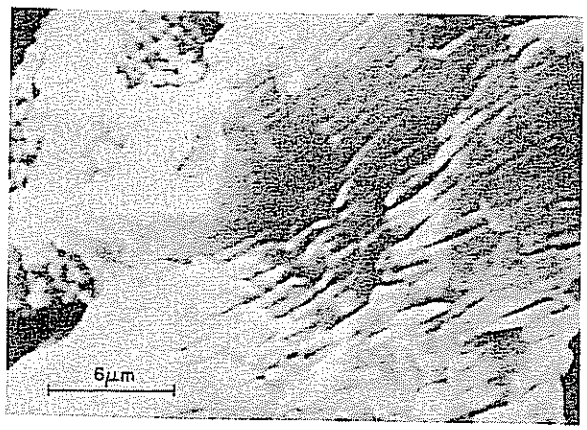

(b)

Fig. 6. (a) Cleavage of filler particles in longitudinal fracture surface of grade 3499 oxidized to a total burn-off of ~20%. (b) Extensive microcracking in transverse fracture surface of grade 3499 oxidized to a total burn-off of ~20%.

primarily occurs by cleavage of the severely degraded filler particles (Fig. 6a), accompanied by regions of inter-particle binder phase failure. In contrast, the crack path lies predominantly (or perhaps entirely) in the binder phase in the tougher transverse orientation for the oxidized samples, in which numerous regions of extensive microcracking are commonly observed (Fig. 6b). No fractured particles are observed in this orientation of the oxidized material. The formation of microcracks, coupled with the extremely tortuous crack path, produces a tougher transverse orientation. Apparently, the tortuous transverse fracture path indicates that the crack is deflected around filler particles, through a binder phase that has been severely weakened by oxidation. In other words, the longer fracture path, accompanied by extensive microcracking, apparently requires less energy than transverse fracture of the oxidized filler particles. In contrast to the transverse fracture morphology in oxidized grade 3499, numerous fractured filler particles were observed in the fractographs of the unoxidized material. This suggests that not only was the binder

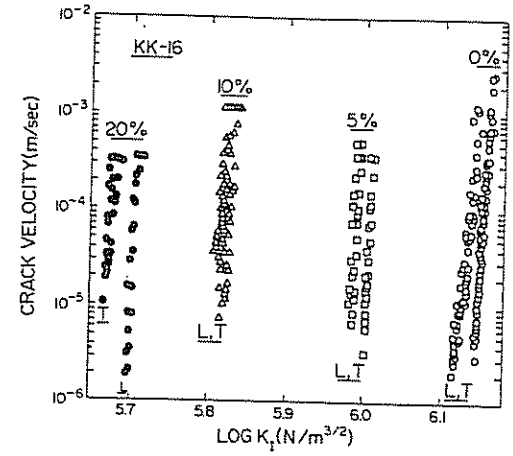

Fig. 7. Isotropic slow crack growth in as-received and oxidized grade KK-16.

phase weakened by oxidation, but that it was preferentially weakened compared to the filler phase.

Despite having the highest fractional internal oxidation of any grade examined (Table 1), the slow crack growth of grade KK-16 was the least affected by the oxidation process. Decreases in the stress intensity necessary for slow crack growth, due to increasing oxidation, are considerably less than the other grades examined. Slow crack growth in grade KK-16 was essentially isotropic at all burn-off levels (Fig. 7). In agreement with the isotropic slow crack growth behavior, there is no apparent difference between the longitudinal (Fig. 8a) and transverse (Fig. 8b) fracture surfaces for grade KK-16, oxidized to 20% weight loss. The micrographs fail to reveal any degradation of the fine-grained filler in this material. The absence of filler particle attack, coupled with numerous observations of exposed filler particles and the absence of binder on the fracture surfaces, indicate that the binder is preferentially oxidized in grade KK-16. No microstructural features were detected which could explain the unusual N-value differences for the longitudinal and transverse specimens oxidized to a 20% weight loss.

Slow crack growth in the lampblack-filled grade 4029 was highly anisotropic for all weight losses, with the transverse orientation consistently tougher than the longitudinal (Fig. 9). Anisotropy in the oxidized material, however, appears to be less pronounced. The fracture path in oxidized grade 4029 is essentially identical to that observed in the as-received material. In the longitudinal orientation, the crack propagates exclusively in the binder phase (Fig. 10a). In the transverse orientation of grade 4029, fracture is a combination of binder phase failure, lampblack aggregate-binder interfacial failure (Fig. 10b) and lampblack aggregate fracture. Qualitatively, fewer fractured aggregates were observed in the oxidized material than in the as-received material. Degradation of the lampblack-binder aggregates appears to be non-uniform with regions of attack corresponding to preferential oxidation of the binder within the aggregates.

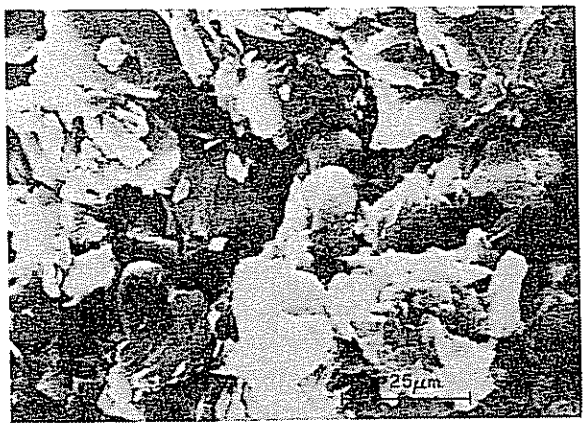

(a)

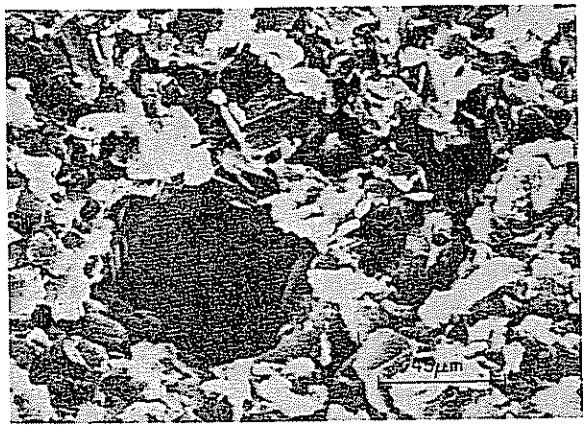

(b)

Fig. 8. (a) Longitudinal fracture surface of grade KK-16 oxidized to a total burn-off of ~20%. (b) Transverse fracture surface of grade KK-16 oxidized to a total burn-off of ~20%.

One intriguing phenomenon observed in this study of crack growth in oxidized graphites is the significant decrease in K_{Ic} observed for only a small amount of internal oxidation at 5% weight loss. If the oxidation reaction occurred totally at the sample surface, one would expect little or no change in crack growth behavior. It has previously been suggested, however, that small amounts of internal oxidation, not readily detected by the apparent density measurements, are occurring in these graphites. The effects of this oxidation on the elastic properties have been documented (Section 3.2) and, in part, mathematically related to microcrack effects on changes in Poisson's ratio. To further examine this phenomenon, transverse specimens of grade 3499 were oxidized at 800°C to 10% burn-off. At this temperature, oxidation is expected to occur almost entirely at the sample surface. The apparent density, moduli and Poisson's ratio of the as-received and oxidized specimens are listed in Table 6. No significant changes are observed for any of the properties of the specimens oxidized at 800°C. Slow crack growth results are presented in Fig. 11. Corresponding K_{Ic} values are listed in Table 6. It is obvious that slow crack growth in the specimens oxidized at 800°C occurs at stress intensities nearly equal to those observed for the as-

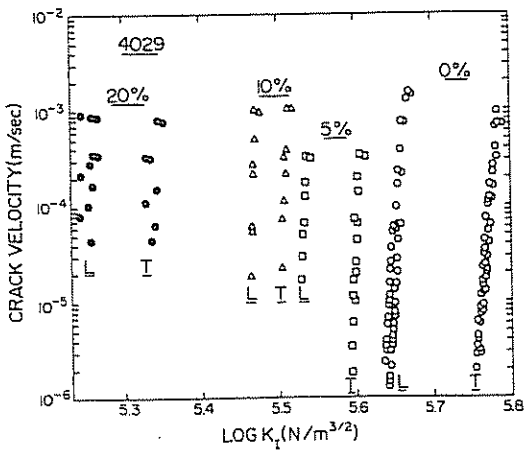

Fig. 9. Anisotropic slow crack growth in as-received and oxidized grade 4029.

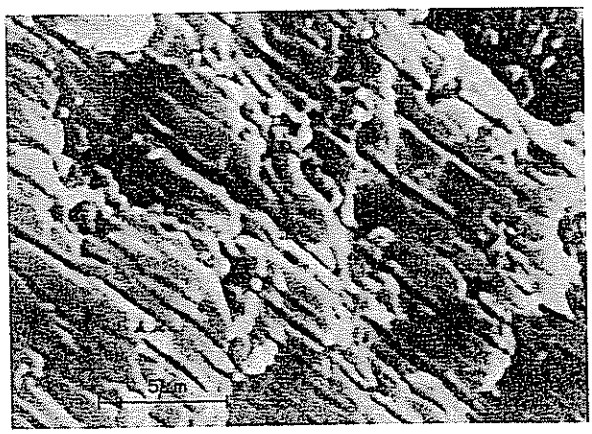

(a)

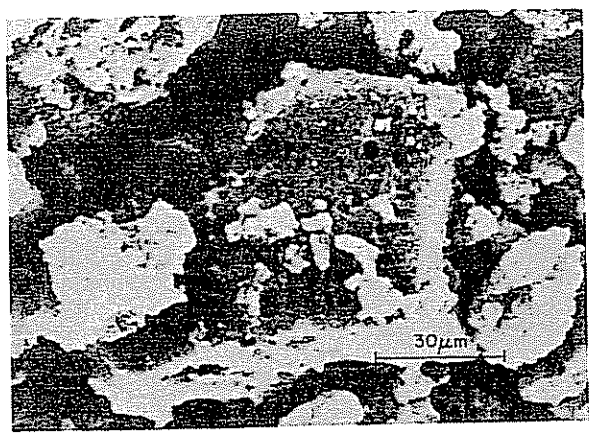

(b)

Fig. 10. (a) Extensive microcracking in longitudinal fracture surface of grade 4029 oxidized to a total burn-off level of ~20%. (b) Lampblack-binder aggregate in transverse fracture surface of grade 4029 oxidized to a total burn-off level of ~20%.

Table 6. Mechanical properties of as-received grade 3499 and samples oxidized at different temperatures

Oxidation Treatment	ρ (gm/cc)	E MN/m^2 (x 10^{-4})	G MN/m^2 (x 10^{-4})	ν	K_{Ic} $MN/m^{3/2}$
As-Received	1.72	0.955	0.429	0.114	1.18
10%-800°C	1.73	0.962	0.429	0.121	1.12
10%-500°C	1.64	0.647	0.289	0.119	0.63

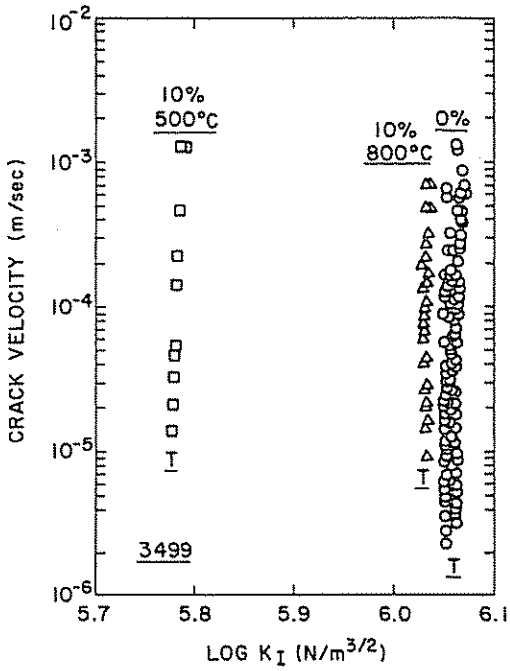

Fig. 11. Slow crack growth in transverse orientation of grade 3499 oxidized to ~10% burn-off at both 500 and 800°C.

received material. In contrast, slow crack growth in the specimens oxidized at 500°C is observed at significantly lower stress intensities. The toughness of the specimens oxidized at 500°C is about one-half of the value for the specimens oxidized at 800°C.

The density, elastic properties, toughness and slow crack growth results indicate that small amounts of internal oxidation significantly decrease the mechanical properties of graphite. When oxidation is confined to the surface, the mechanical properties are virtually unaltered.

4. CONCLUSIONS

The effects of oxidation on the fracture toughness and subcritical crack growth of four commercial polycrystalline graphites were studied at room temperature. Fracture toughnesses decreased markedly with increasing oxidation. Exponential decreases in elastic moduli as well as decreases in the fracture surface energy contributed to lowering K_{Ic}. These decreases in K_{Ic} can explain most of the strength reductions noted in previously published studies of oxidized graphites. Only a single (K_I–V_I) region was observed, always at large fractions of the respective K_{Ic}'s, suggesting that slow crack growth is primarily governed by mechanical fracture processes.

Oxidation generally shifts the single (K_I–V_I) region to lower stress intensity factors and decreases the slope to lower N-values. A combination of filler particle and binder phase degradation during oxidation is responsible for these decreased K_I and N-values. Where studied, oxidation reduces slow crack growth anisotropy.

Changes in the oxidation conditions can significantly affect the magnitude of the decreases in the physical, elastic and mechanical properties of graphites.

Acknowledgements—This study was made possible by a fellowship grant from the Airco Speer Carbon-Graphite Co., St. Marys, PA. Discussions with P. Thrower, H. Goochee, and F. Fair are gratefully acknowledged. R. Pysz of Airco Speer Carbon–Graphite was helpful in interpreting SEM results, particularly on the lampblack-binder aggregates.

REFERENCES

1. A. A. Griffith, *Phil. Trans. Roy Soc.* **A221**, 163 (1920).
2. A. C. Collins, H. G. Masterson and P. P. Jennings, *J. Nucl. Mater.* **15**, 135 (1965).
3. J. A. Board and R. L. Squires, *Proc. 2nd Conf. on Ind. Carbon and Graphite*, p. 289. Soc. Chem. Ind., London (1966).
4. C. Rounthwaite, C. A. Lyons and R. A. Snowdon, *Proc. 2nd Conf. on Ind. Carbon and Graphite*, p. 299. Soc. Chem. Ind., London (1966).
5. R. H. Knibbs and J. G. Morris, *Proc. 3rd Conf. on Ind. Carbon and Graphite*, p. 297. Soc. Chem. Ind., London (1971).
6. J. C. Bognet, M.S. Thesis, The Pennsylvania State University (1977).
7. J. L. Wood, R. L. Bradt and P. L. Walker Jr., *Carbon* to be published.
8. J. O. Outwater, M. C. Murphy, R. G. Kumble and J. T. Berry, *Fracture Toughness and Slow-Stable Cracking*, ASTM STP 559, American Society for Testing and Materials, 127 (1974).
9. P. L. Walker Jr., F. Rusinko Jr. and L. G. Austin, *Advances in Catalysis*, Vol. XI. Academic Press, New York (1959).
10. S. Spinner and W. E. Tefft, *ASTM Proc.* **61**, 1221 (1961).
11. B. Budiansky and R. J. O'Connell, *Int. J. Solid Struct.* **12**, 81 (1976).

12. J. R. Cost, K. R. Janowski and R. C. Rossi, *Phil. Mag.* **17**, 851 (1968).
13. O. L. Blakslee, D. G. Proctor, E. J. Seldin, G. B. Spence and T. Weng, *J. Appl. Phys.* **41**, 3373 (1970).
14. W. Voigt, *Lehrbuch der Kristallphysik*. Teubner, Leipzig (1928).
15. A. Reuss, *Z. Angew. Math. Mech.* **9**, 49 (1929).
16. S. W. Freiman and J. J. Mecholsky, *REVMAT Quart. Prog. Rep.* (Mar. 1975).
17. R. B. Bruce, *J. Metal Club*, R. G. S. Glasgow, No. 10, 41 (1958–59).
18. R. J. Good, L. A. Girifalco and G. Kraus, *J. Phys. Chem.* **62**, 1418 (1958).
19. J. S. Nadeau, *J. Am. Ceram. Soc.* **57**, 303 (1974).